Hindawi
Mathematical Problems in Engineering
Volume 2020, Article ID 8843657, 11 pages
https://doi.org/10.1155/2020/8843657

Research Article

Layout Design of Stiffened Plates for Large-Scale Box Structure under Moving Loads Based on Topology Optimization

Zhaohua Wang[1], **Chenglong Yang**[1], **Xiaopeng Xu**[2], **Dezhuang Song**[1] and **Fenghe Wu**[1,3]

[1]*School of Mechanical Engineering, Yanshan University, Qinhuangdao 066004, China*
[2]*School of Mechanical Engineering, Luoyang Institute of Science and Technology, Luoyang 471023, China*
[3]*Heavy-Duty Intelligent Manufacturing Equipment Innovation Center of Hebei Province, Qinhuangdao 066004, China*

Correspondence should be addressed to Fenghe Wu; risingwu@ysu.edu.cn

Received 1 October 2020; Revised 27 October 2020; Accepted 28 October 2020; Published 10 November 2020

Academic Editor: Ponnusamy Venkumar

Copyright © 2020 Zhaohua Wang et al. This is an open access article distributed under the Creative Commons Attribution License, which permits unrestricted use, distribution, and reproduction in any medium, provided the original work is properly cited.

As the main load-bearing structure of heavy machine tools, cranes, and other high-end equipment, the large-scale box structures usually bear moving loads, and the results of direct topology optimization usually have some problems: the load transfer skeleton is difficult to identify and all working conditions are difficult to consider comprehensively. In this paper, a layout design method of stiffened plates for the large-scale box structures under moving loads based on multiworking-condition topology optimization is proposed. Based on the equivalent principle of force, the box structures are simplified into the main bending functional section, main torsional functional section, and auxiliary functional section by the magnitude of loads and moments, which can reduce the structural dimension and complexity in topology optimization. Then, the moving loads are simplified to some multiple position loads, and the comprehensive evaluation function is constructed by the compromise programming method. The mathematical model of multiworking-condition topology optimization is established to optimize the functional sections. Taking a crossbeam of superheavy turning and milling machining center as an example, optimization results show that the stiffness and strength of the crossbeam are increased by 17.39% and 19.9%, respectively, while the weight is reduced by 12.57%. It shows that the method proposed in this paper has better practicability and effectiveness for large-scale box structures.

1. Introduction

The large-scale box structures are widely used in heavy equipment such as machine tools, cranes, and so on. They usually bear the moving loads with the continuous change of position and its stiffness, strength, and weight directly affect the mechanical performance of the equipment. For example, the crossbeam of a machine moves on the gantry and bears the loads from the cutting components. The stiffness directly affects the machining accuracy [1]. The main beam of a large bridge crane bears the moving loads when carrying goods, it moves on the end beam (fixed on the wall), and the strength directly affects the safety of the lifting process [2]. At present, the experience analogy method is mainly used in the design of the large-scale box structures, but the structures are always cumbersome because of the large safety factor, which causes large inertial loads and affects the operation sensitivity. Therefore, the design of large-scale box structures with high stiffness, high strength, and low weight is the long-term goal of engineers.

The box structures are composed of external skin and internal stiffened plates, and the essence of lightweight design is to optimize the layout and size parameters of the internal stiffened plates [3]. At present, the researches on the layout optimization of two-dimensional (2D) stiffened plates have been widely concerned by many scholars [4–6], while the research on the large-scale three-dimensional (3D) box structures is very few. Some scholars try to realize the lightweight design of the box structures by means of structural bionics. Gao et al. [7, 8] studied the distribution law of the main vein and the secondary vein in the leaf vein, and the bionic design of the internal stiffened plates of a

machine tool column was carried out to improve the structural performance based on the principle of similarity. But the design idea is subjective in the selection of the biological prototype as well as structural design, which lacks a theoretical basis. In references [9–12], a method for optimizing the layout of stiffened plates in the box structures is proposed according to the growth mechanism of the biological branching system in nature. The stiffened plates grow, bifurcate, and degenerate towards the direction of the maximum total stiffness under the given loads and constraints, and the layout with an effective load path is obtained. However, the layout calculated is complex; the processing cost is very high, especially for the large-scale box structures with the moving loads.

Topology optimization is a method that is used to seek an optimal configuration for the hollow location and number in some certain and continuous regions. It has been widely used in structural lightweight design [13–15], and some scholars apply topology optimization to the layout optimization of 3D box structure. Qin and Zhu [16] established a topology optimization model based on the method of moving asymptotes for the bridge crane girder structures, and some satisfying results were obtained. However, the method is only suitable for the discrete box girder structures and cannot be applied to the continuum structures studied in this paper. Konstantinos et al. [17] focused on the application of structural topology optimization to design steel perforated I-sections to replace the traditional cellular beams, and an optimum web opening configuration was suggested. But the applied load is uniform and invariable, and the beam section can be equivalent to the 2D structures, which cannot be applied to the 3D box structures. Young-Sop et al. [18] proposed a reliability-based topology optimization for the 3D structures using bidirectional evolutionary structural optimization and the standard response surface method. The results show that the optimal topology obtained for the 2D and 3D cantilever beams is very similar, and the thickness of the optimal topology gradually increased from the free end to the fixed end. However, due to the large aspect ratio of the large-scale box structures, the 3D topology optimization directly is easy to generate material aggregation [19, 20] and the inclined beam [21], resulting in the problems of difficult identification of the optimization results, which cannot be manufactured by traditional machining. The Additive Manufacturing (AM) can manufacture the structures with complex features, but it is still limited by the size and technology [22] and cannot be applied to the large-scale 3D box structures. On the other hand, the large-scale box structures usually bear the moving loads with the continuous change of position. The optimizations of extreme working conditions are easy to cause the problem of load sickness [23, 24].

Based on the above problems, this paper proposes a layout design method for the large-scale box structures under moving loads based on multiworking-condition topology optimization, which transforms the 3D topology optimization with moving loads of the large-scale box structures into the 2D topology optimization with multiple position loads. Section 2 describes the existing problems of topology optimization for large-scale box structures. The design method of structural decomposition process based on the functional sections and multiworking-condition topology optimization are introduced, respectively, in Section 3. Then, a crossbeam of a superheavy turning and milling machining center is taken as a case study and optimized by the proposed method.

2. Problem

2.1. SIMP Topology Optimization. SIMP topology optimization [25, 26] is a common method for topology optimization of the continuum structures, which introduces a material with a hypothetical relative density varying between 0 and 1 and uses a penalty factor to disperse the intermediate density value to 0/1, so as to eliminate the elements with intermediate density. In this paper, the optimal topology with maximum stiffness is calculated under the constraint of a certain material removal rate based on the theory of SIMP topology optimization. A topology optimization problem with the maximum stiffness as the objective can be expressed as follows:

$$\begin{cases} \text{find } x = (x_1, \ldots, x_n), \\ \min c(x) = \mathrm{U}^T \mathbf{K} \mathrm{U} = \sum_{e=1}^{n} (x_e)^p \mathbf{u}_e^T \mathbf{K}_e \mathbf{u}_e, \\ \text{subject to } \mathbf{K}(x)\mathbf{u} = F, \\ V(x) \le f \cdot V_0, \\ 0 < x_{\min} \le x_e \le 1, \end{cases} \tag{1}$$

where x is the relative density, $c(\mathrm{x})$ is the structural compliance; p is the penalty factor, $p > 1$. $\mathbf{U}$ and $\mathbf{F}$ are the displacement vector and the force vector. $\mathbf{K}(x)$ is the stiffness matrix of FEM. $\mathbf{u}_e$ and $\mathbf{K}_e$ are the displacement vector and stiffness matrix corresponding to the eth element. $V(x)$ is the objective volume value and V_0 is the initial volume value. $x_{\min}$ and x_e represent the minimum of relative density and the relative density of eth element, respectively, f is the prescribed volume fraction.

The optimization problem could be solved using several different approaches, such as Optimality Criteria (OC) methods, Sequential Linear Programming (SLP) methods, or the Method of Moving Asymptotes (MMA) and others [27]. For simplicity, we will here use a standard OC-method in this paper. Following Bendsøe [28], a heuristic updating scheme for the design variables can be formulated as follows:

$$x_e^{\text{new}} = \begin{cases} a, & \text{if } x_e B_e^{\eta} \le a, \\ x_e B_e^{\eta}, & \text{if } a < x_e B_e^{\eta} < b, \\ b, & \text{if } b \le x_e B_e^{\eta}. \end{cases} \tag{2}$$

where $a = \max(x_{\min}, x_e - m)$, $b = \min(1, x_e + m)$, m is a positive move-limit, η is a numerical damping coefficient, and B_e is found from the optimality condition as follows:

$$B_e = \frac{-(\partial c / \partial x_e)}{\lambda (\partial V / \partial x_e)}, \tag{3}$$

where λ is a Lagrangian multiplier that can be found by a bisectioning algorithm. The sensitivity of the objective function is found as follows:

$$\frac{\partial c}{\partial x_e} = -p\left(x_e\right)^{p-1} \mathrm{u}_e^T \mathrm{k}_0 \mathrm{u}_e. \tag{4}$$

2.2. Topology Optimization of a Box Structure. A large number of stiffened plates are usually arranged in the large-scale box structures to improve the stiffness and strength, so the essence of lightweight is to optimize the layout of stiffened plates. Taking a typical box structure with $1000 \times 200 \times 200$ mm shown in Figure 1 as an example, the left and right ends are fixed, and a vertical downward load F is applied on the left side of the upper face in Case 1, while F is applied in the middle of the upper face in case 2. The SIMP method (equations (1)–(4)) is used to calculate the load transfer skeleton in the box structure under two working conditions, and the results are shown in Figure 2.

Due to the large aspect ratio of the structure shown in Figure 1, the results show that there is a serious material deposition after topology optimization of two working conditions, and the result of case 2 appears inclined rib plates in three dimensions, which brings great trouble to the manufacturing. In addition, it can be seen from the comparison between Figures 2(a) and 2(b) that the load transfer skeletons under two working conditions are completely different because of the applied load in a different position. So, it is difficult to guarantee the safety of other working conditions if only the extreme working condition is considered, which may result in the problem of load sickness [29].

Therefore, we can get a conclusion: the direct topology optimization of the large-scale box structures has some problems: the load transfer skeletons are difficult to identify and all working conditions are difficult to consider comprehensively, which cannot provide guidance for the rational layout design of the internal stiffened plates. So, it is necessary to develop new design ideas to optimize large-scale box structures.

3. Method

According to the above problems, we assume that the material redundancy problem may be solved if we convert the 3D topology optimization problem into a 2D problem. The moving loads can be simplified to multiple position loads, which will restore the actual working condition of the box structures.

3.1. Decomposition of the Functional Section. The decomposition method of the functional sections refers to a method of decomposing the complex 3D structure into 2D sections by analyzing loads of complex working conditions. For the structures with complex working conditions, the loads can be simplified according to the equivalent principle of force in theoretical mechanics. As shown in Figure 3, the Cartesian coordinate system is established by selecting a

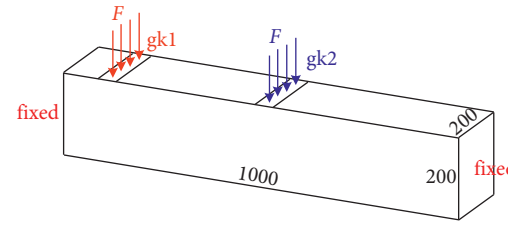

Figure 1: Diagram of a large-scale box structure.

point on the structure (such as the center of mass) as the origin, and then the spatial force system is simplified to this point so that the loads (F_x, F_y, F_z) and moments (M_x, M_y, M_z) are decomposed into three coordinate axes.

For the convenience of calculation, the XY plane, XZ plane, and YZ plane are defined as 2D functional sections, and the loads corresponding to each functional section are calculated and sorted. Take the plane with the largest load as the main bending functional section and the plane with the largest moment as the main torsional functional section. For example, if $F_x > F_y > F_z$, the XY plane is defined as the main bending functional section and the XZ plane as the secondary bending functional section. If $M_x > M_y > M_z$, the YZ plane is defined as the main torsional functional section and the XZ plane as the secondary torsional functional section. The last plane is the auxiliary functional section.

After determining the functional sections, the bearing types and boundary conditions of each functional section are analyzed and simplified. The Finite Element Model (FEM) is established, and topology optimization can be carried out by equation (1). So, the topology optimization of the large-scale box structures is transformed into the topology optimization of 2D functional sections. Finally, the 3D reconstruction of the topology optimization results of each functional section is carried out to obtain a lightweight 3D box structure.

3.2. Topology Optimization under the Moving Load. In this paper, the moving loads on the large-scale box structures are equivalent to several working conditions according to the position of loads. It is necessary to unify the optimization objectives of each working condition to consider the load transfer skeletons at any position in the process of topology optimization, which is a problem of multiobjective topology optimization.

A comprehensive evaluation function is needed to transform the multiobjective problem into a single objective problem. The linear weighting method is usually used to make it in the traditional multiobjective topology optimization. But it is to calculate weight average value for all functions and cannot reflect the prominent influence from some certain functions, which does not guarantee that all functions obtain the relative optimal solutions. The compromise programming method [30] can get a group of a better relative optimal solution by calculating the sensitivity of all functions to design variables and adjusting each objective to balance each other.

So, the objective function of the static multiworking-condition stiffness is established by the compromise

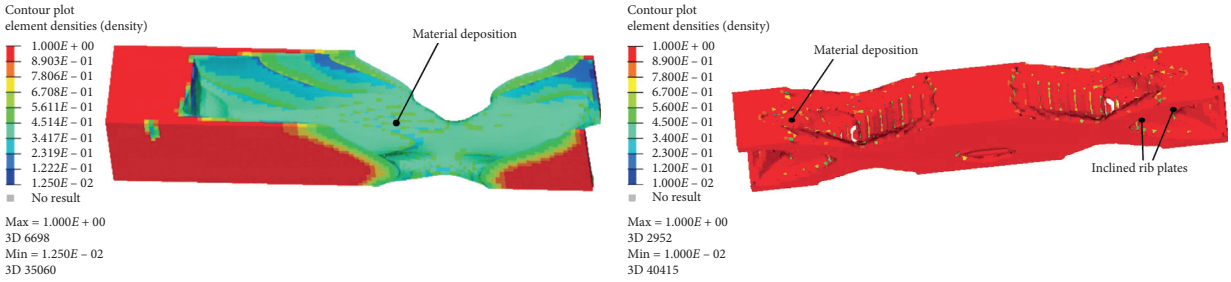

Figure 2: Optimization results. (a) Case 1, (b) case 2.

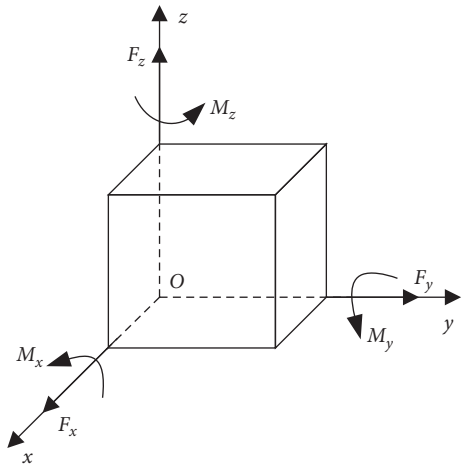

Figure 3: Diagrammatic sketch of load equivalent.

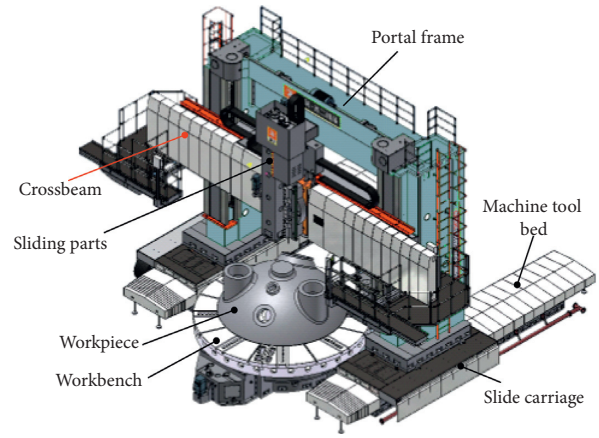

Figure 4: Superheavy turning and milling machining center.

programming method, as shown in equation (5). $C(x)$ is the comprehensive evaluation value of the static stiffness, and the smaller the value, the larger the structural overall stiffness.

$$\min_x C(x) = \left\{ \sum_{i=1}^{n} \omega_i^q \left[\frac{C_i(x) - C_i^{\min}}{C_i^{\max} - C_i^{\min}} \right]^q \right\}^{(1/q)}, \quad (5)$$

where n is the total number of working conditions. w_i is the weight coefficient of the ith working condition while q is the penalty coefficient ($q \geq 2$). $C_i(\rho)$ is the structural compliance of the ith working condition. $C_i^{\max}$ and $C_i^{\min}$ are the maximum and minimum compliance of the ith working-condition, respectively.

4. Topology Optimization of Crossbeam

In this paper, a large-scale crossbeam of superheavy turning and milling machining center is taken as an example to verify the proposed method. The turning and milling machining center is composed of crossbeam, sliding parts, workbench, slide carriage, machine tool bed, portal frame, and other components, as shown in Figure 4.

The crossbeam is installed on the portal frame, which is the supporting part of the sliding parts and also the main part bearing the cutting forces. Its static and dynamic performance directly affects the accuracy of the machine tool. The crossbeam is 10.4 m long, 7.5 m span, 1.28 m wide, 1.8 m high, and 40058 kg weight, and it is welded by a Q235 steel plate. It belongs to a typical box structure because of its large volume and mass, large inertia load in the process of moving up and down. To improve the overall mechanical performance of the crossbeam, the decomposition method of functional sections and multiworking-condition topology optimization are used to optimize the layout of the internal stiffened plates.

4.1. Finite Element Analysis. The crossbeam and sliding parts not only contain many parts but also have complex features. The efficiency and accuracy of the Finite Element Analysis (FEA) for all parts are very low, which is easy to lead to errors in simulation analysis. In order to improve the calculation efficiency, the features such as small holes, small corners, small gaps, and welds on the crossbeam are ignored, and a simplified model is established, as shown in Figure 5. According to the moving range of the sliding parts on the guide rail (0~7400 mm), taking the distance from the slider to the right boundary of the crossbeam as reference distance, 11 positions of the sliding parts along Y-direction are selected for FEA. When the sliding parts are in 3700 mm along Y direction, they are located at the middle of the crossbeam.

The boundary condition of the crossbeam can be equivalent to a simply supported beam. The sliding parts

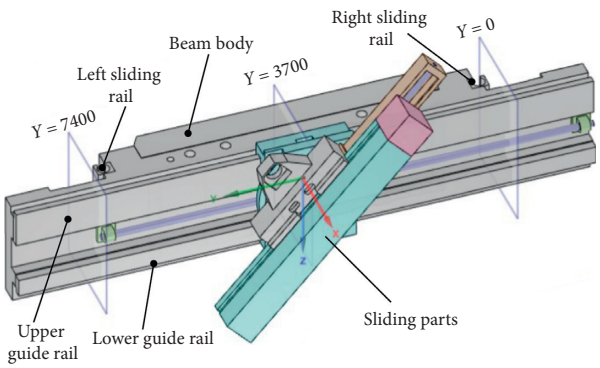

Figure 5: Simplified model of the crossbeam.

slide on one side of the crossbeam, and the crossbeam bears offset moving loads. Therefore, the loads that cause deformation of the crossbeam include self-gravity, gravity of the sliding parts, distortion caused by offset loads, and cutting forces. The cutting forces of the turning and milling machining center under a typical working condition are shown in Table 1. Since the cutting forces are much smaller than the self-gravity (400580 N), only the deformation caused by gravity is regarded as the static characteristics of the crossbeam. In addition, the rotation of the sliding parts is not considered because it has little influence on the static response of the crossbeam. The displacement constraints are applied to the crossbeam: X-direction constraint is applied to the large guide rail surface of the crossbeam and the portal frame (DOF_ X in Figure 6), Y-direction constraint is applied to the small guide rail surface of the crossbeam and the portal frame (DOF_ Y in Figure 6), and Z-direction constraint is applied to the left and right screw holes (DOF_ Z in Figure 6).

The model is imported into the FEA software ANSYS. The tetrahedral element is used to divide the parts with complex features, while the hexahedral element (hexdominant method) is used to divide other parts. The loads and constraints shown in Figure 6 are applied and the FEM is shown in Figure 7 (Y = 3700 mm).

As the sliding parts move to different positions on the crossbeam, the static response is different. 11 key positions are selected along the Y-direction for FEA, and the response curve of static maximum displacement is shown in Figure 8. The curve clearly reflects that the displacement of the crossbeam increases first, then decreases, and then increases from 0 to 7400 mm in Y-direction. When the sliding parts move to the middle of the crossbeam ($Y = 3700$ mm), the maximum deformation is 0.1289 mm, and the corresponding displacement distribution is shown in Figure 9(a). At this position, the stress distribution is shown in Figure 9(b), and the maximum stress is 12.77 MPa, which is less than the material yield strength (235 MPa). Therefore, it can be seen that the overall stress value of the crossbeam is relatively small, and there is a large lightweight space.

4.2. Establish Functional Sections. In this section, the decomposition method of functional sections is used to reduce

Table 1: Cutting forces under a typical working condition.

	Main cutting force F_c	Feeding force F_f	Radial force F_r
Value (N)	74760	41118	29904

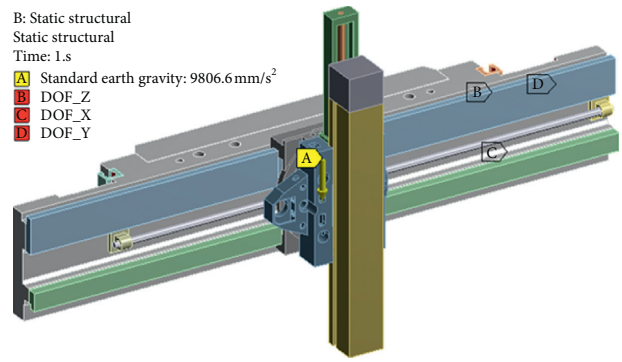

Figure 6: Simplified boundary conditions of the crossbeam.

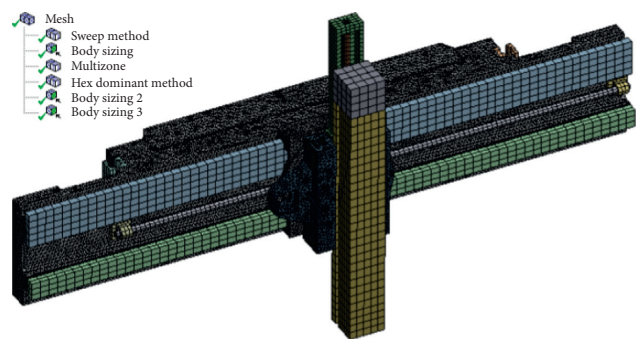

Figure 7: Finite element model ($Y = 3700$ mm).

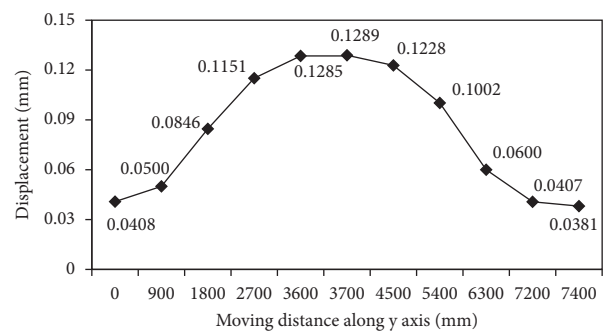

Figure 8: The response curve of the static maximum displacement.

the dimension of the crossbeam in topology optimization. Firstly, the coordinate system (shown in Figure 10) is established with the center of mass of the crossbeam as the origin.

According to the equivalent principle of force, loads of the crossbeam under the typical cutting condition mainly include self-gravity G_1, gravity G_2 of the sliding parts, cutting forces (main cutting force F_c, radial force F_r, feeding force

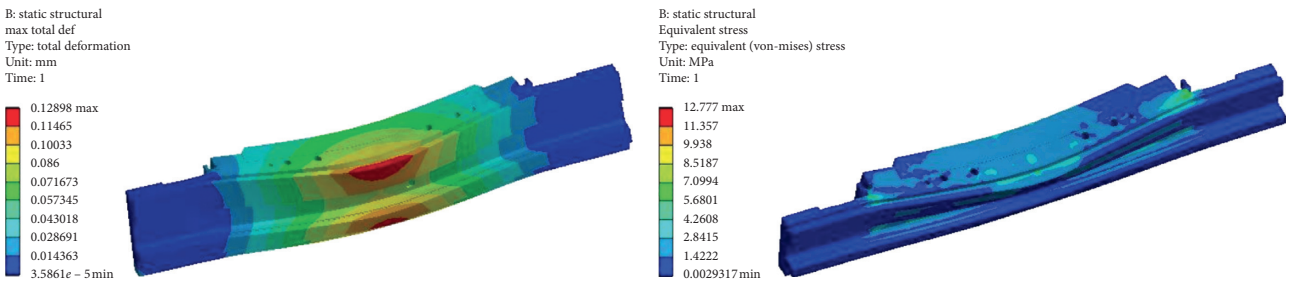

Figure 9: The results of FEA ($Y = 3700$ mm). (a) Displacement distribution. (b) Stress distribution.

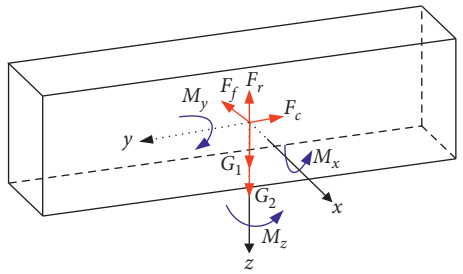

Figure 10: Equivalent loads at the center of mass of the crossbeam.

F_f), and moments $M_x \backslash M_y \backslash M_z$ from above loads on the center of mass. It can be seen from Section 4.1 that the gravity of the crossbeam and the sliding parts is far greater than the cutting forces and $F_c > F_f > F_r$ (Table 1). Therefore, it is obvious from Figure 10 that the equivalent loads at the center of mass have a relationship as follows:

$$\begin{cases} F_z > F_y > F_x, \\ M_y > M_x > M_z. \end{cases} \tag{6}$$

Based on the principle of determining functional sections proposed in Section 3, the YZ plane is defined as the main bending functional section, the XZ plane is defined as the main torsional functional section (also the secondary bending functional section), and the XY plane is defined as the auxiliary functional section. As the main function of the crossbeam is to resist overall bending deformation and torsional deformation caused by the offset loads, the main bending functional section and the main torsional functional section are only selected for topology optimization.

The main bending functional section is shown in Figure 11(a). As the sliding parts slide on the guide rail of the crossbeam, and the guide rail is not taken as the optimization object. So, the length that can be optimized is less than the length of the guide rail, and the size is set as $6850 \times 1580 \times 10$ mm. The moving load is equivalent to nine working conditions with the same distance, as shown in Figure 11(b). When the load is at different positions of the section, there are significant differences in the load transfer skeleton by topology optimization. So, it is necessary to carry out multiworking-condition topology optimization for the main bending functional section.

The main torsional functional section is shown in Figure 12(a). The torsional load mainly comes from the pressure exerted by the sliding parts on the guide rail, and the section shape is complex. So, the sectional size is simplified to a cube of $1000 \times 1000 \times 20$ mm, and the equivalent working condition is shown in Figure 12(b).

4.3. Topology Optimization

4.3.1. Main Bending Functional Section. In this section, topology optimization of the main bending functional section under nine working conditions ($n = 9$ in fd5(5)) is carried out. It is necessary to first determine the weight coefficient w_i of nine working conditions when establishing the comprehensive evaluation function of the crossbeam. According to the deformation law of the simply supported beams in theoretical mechanics, the closer the concentrated force is to the middle position, the larger the deformation is. In this paper, the response curve of displacement shown in Figure 8 is taken as the index, and the weight coefficients of each working condition are set as 0.07, 0.08, 0.1, 0.15, 0.2, 0.15, 0.1, 0.08, 0.07.

In addition, $C_i^{\max}$ and $C_i^{\min}$ in equation (5) are the maximum and minimum compliance of the ith working-condition, respectively, which can be obtained from the single-working-condition topology optimization. Therefore, the FEM of nine working conditions are established, respectively, and the single-working-condition topology optimization is carried out with equation (1). The results of $C_i^{\max}$ and $C_i^{\min}$ are shown in Table 2.

Taking the relative density as the design variable and a material removal rate of 30% as the constraint condition, aiming at the minimum comprehensive evaluation value of the static stiffness under multiple working conditions, the mathematical model of multiworking-condition topology optimization is established as shown in the following equation:

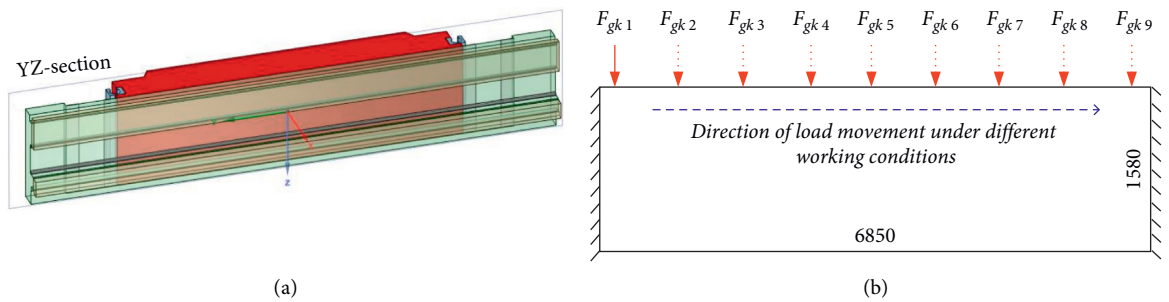

Figure 11: Main bending functional section. (a) YZ plane. (b) Equivalent working condition.

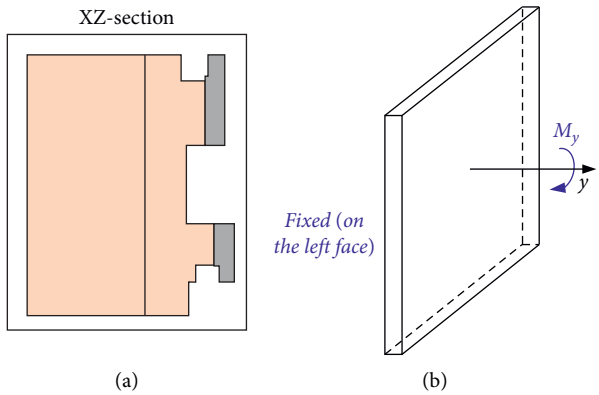

Figure 12: Main torsional functional section. (a) XZ plane, (b) equivalent working condition.

Table 2: The compliance of the ith working condition (Nmm).

No.	1	2	3	4	5	6	7	8	9
$C_k^{\min}$ (Nmm)	2.66	4.07	6.14	8.69	9.82	8.69	6.14	4.08	2.67
$C_k^{\max}$ (Nmm)	10.39	14.23	18.26	21.38	22.55	21.38	18.26	14.23	10.39

$$\begin{cases} \text{find } x = (x_1, \ldots, x_n), \\ \min C(\rho) = \left\{ \sum_{i=1}^{9} \omega_i^2 \left[\dfrac{C_i(\rho) - C_i^{\min}}{C_i^{\max} - C_i^{\min}} \right]^2 \right\}^{(1/2)}, \\ \text{subject to } \mathbf{K}(x)\mathbf{u} = \mathrm{F}, \\ V(x) \le 0.7 \cdot V_0, \\ 0 < x_{\min} \le x_e \le 1. \end{cases} \tag{7}$$

The optimization result is shown in Figure 13, and the importance degree of each region is decreasing when the color changes from red to blue. The load transfer skeleton of the YZ section is clearly given and the stiffened plates are established as shown in Figure 14.

In order to show the advantages of multiworking-condition topology optimization, the topology optimization of the fifth working condition (F_{gk5} in Figure 11(b)) is calculated. The result (Figure 15) shows that the load transfer skeleton can well bear the loads under the fifth working condition, but it is obvious that the layout of the stiffened

Figure 13: The optimization result.

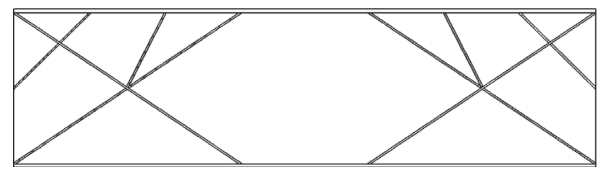

Figure 14: The layout of internal stiffened plates.

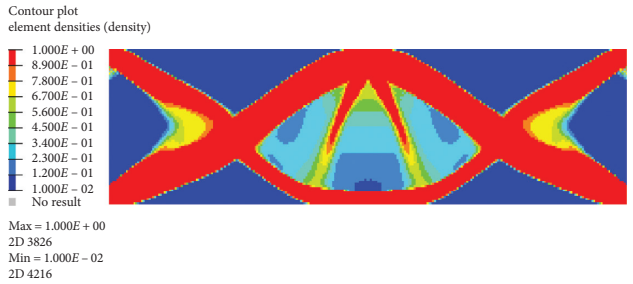

Figure 15: Optimization result of the fifth working condition.

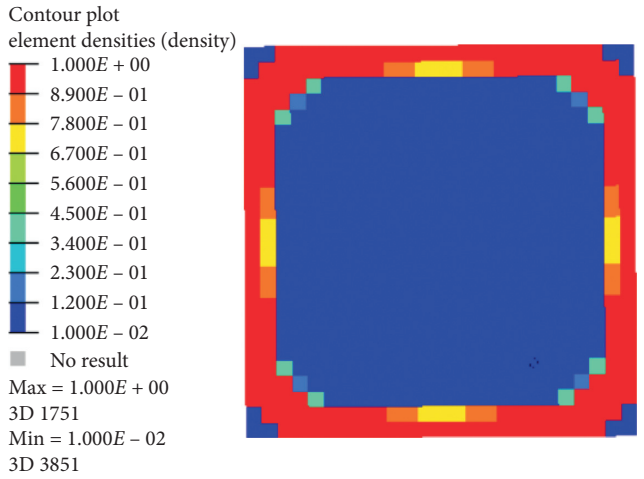

Figure 16: The optimization result of the XZ section.

plates is not suitable for other working conditions. On the contrary, the result of Figure 13 shows multiple stiffened plates at the location where the load is applied at the upper boundary of the functional section, which can meet the loads generated by the sliding parts at different locations of the crossbeam. Therefore, the result of Figure 13 is better than that of Figure 15.

4.3.2. Main Torsional Functional Section. The results of topology optimization for a main torsional functional section are shown in Figure 16, which shows that the best shape of a rectangular section is hollow and the corners are chamfered. So, the feature of chamfer is added to the cross section of the crossbeam in XZ plane, as shown in Figure 17.

Based on the above results, the new model of the crossbeam is established as shown in Figure 18.

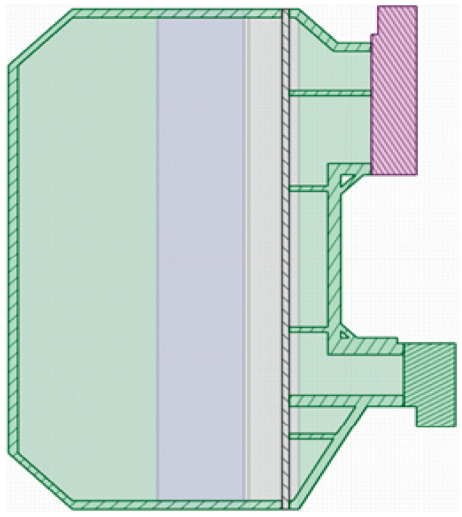

Figure 17: New cross section of the crossbeam.

4.4. Verification of Optimization Result. In order to verify the effect of multiworking-condition topology optimization of the crossbeam, taking the new model as the research object and applying the same boundary conditions (the same as Figure 6), the displacement of 11 working conditions is analyzed by FEA again. The total displacement response is shown in Table 3, and the comparison curve is shown in Figure 19.

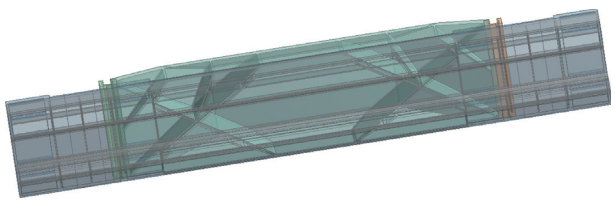

Figure 18: The new model of the crossbeam.

Table 3: The displacement of 11 working conditions.

No.	1	2	3	4	5	6	7	8	9	10	11
Location Y (mm)	0	0.04083	0.03227	2700	3600	3700	4500	5400	6300	7200	7400
Initial model (mm)	900	0.04998	0.04182	0.11514	0.12850	0.12898	0.12279	0.10020	0.06001	0.04068	0.03808
New model (mm)	1800	0.08456	0.07074	0.09542	0.10642	0.10655	0.09726	0.07365	0.04323	0.03319	0.03259

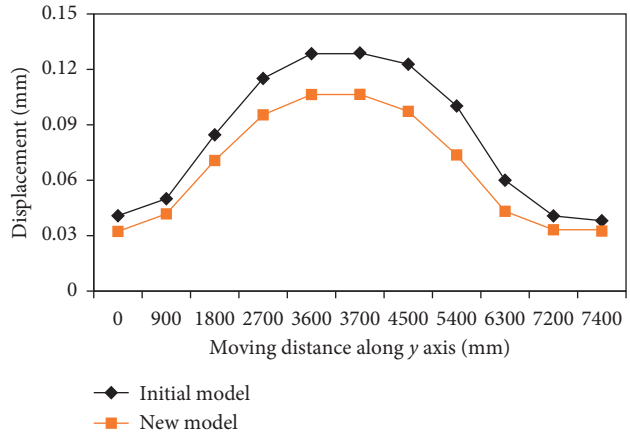

Figure 19: The comparison of the displacement response.

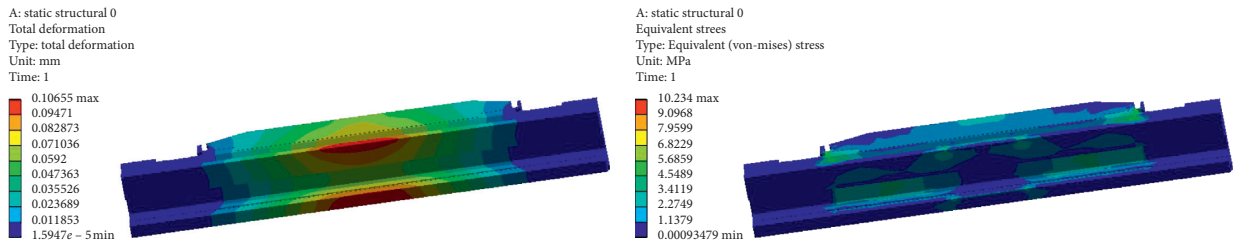

(a) (b)

Figure 20: The results of FEA for the new model. (a) Displacement distribution. (b) Stress distribution.

The results show that the overall displacements of the crossbeam become smaller than the initial model, which indicates that the structural stiffness is strengthened. Figure 19 also shows that the total deformation of the new model is largest when the sliding parts are at the middle of crossbeam ($Y = 3700$ mm). The displacement and stress distribution under extreme working conditions are shown in Figure 20. The maximum displacement is 0.10655 mm, which is 17.39% lower than the initial model, indicating that the static stiffness of the crossbeam has been significantly improved. The maximum stress is 10.234 MPa, which is smaller than the material yield strength (235 MPa), meeting the strength requirements.

Compare the static mechanical performances when the sliding parts are in the middle of crossbeam ($Y = 3700$ mm), as shown in Table 4. It can be seen that the maximum displacement value of the new crossbeam is reduced by 17.39%, the maximum stress value is reduced by 19.9%, and the mass is changed from 40058 kg to 35023 kg, which is reduced by 12.57%, indicating that the lightweight effect is very good.

Table 4: Comparison of mechanical performances.

	Max displacement (mm)	Max stress (MPa)	Mass (kg)
Initial model	0.12898	12.777	40058
New model	0.10655	10.234	35023
Variation	−17.39%	−19.9%	−12.57%

5. Conclusions

In this paper, a layout design method for the large-scale box structures under moving loads based on multiworking-condition topology optimization is proposed to solve the problem of difficult identification and complex moving loads. According to the magnitude of loads and moments, the complex 3D structure is transformed into 2D functional sections including the main bending functional section, the main torsional functional section, and the auxiliary functional section, which makes the topology optimization simplify from 3D to 2D. The complex moving loads are equivalent to several working conditions, and the

comprehensive evaluation function is constructed by using the compromise programming method, which solves the problem of load sickness under the topology optimization of extreme single-working-condition and avoids that the result is only the local optimal solution rather than the global optimal solution. Taking a crossbeam of superheavy turning and milling machining center as an example, the optimization results show that the stiffness and strength of the crossbeam are increased by 17.39% and 19.9%, respectively, while the weight is reduced by 12.57%. It shows that the method proposed in this paper has better practicability and effectiveness for large-scale box structures.

Data Availability

The data can be obtained from the corresponding author.

Conflicts of Interest

The authors declare that they have no financial and personal relationships with other people or organizations that can inappropriately influence their work, and there is no professional or other personal interest of any nature or kind in any product, service, and/or company that could be construed as influencing the position presented in this manuscript.

Acknowledgments

This work was supported by the Chinese National Key Research and Development Program (2016YFC0802900) and the Key Natural Science Projects of Hebei Provincial Department of Education (ZD2020156).

References

[1] S. Liu, Y. Li, Y. Liao, and Z. Guo, "Structural optimization of the cross-beam of a gantry machine tool based on grey relational analysis," *Structural and Multidisciplinary Optimization*, vol. 50, no. 2, pp. 297–311, 2014.

[2] Q. X. Wang, X. F. Zhang, and C. B. Sun, "Lightweight design and research of box girder for double girder bridge crane," *Applied Mechanics and Materials*, vol. 229–231, pp. 478–481, 2012.

[3] C. Sun, T. Ying, J. C. Zeng, J. S. Pan, and Y. F. Tao, "The structure optimization of main beam for bridge crane based on an improved PSO," *Journal of Computers*, vol. 6, no. 8, pp. 1585–1590, 2011.

[4] H. Huang, H. An, H. Ma, and S. Chen, "An engineering method for complex structural optimization involving both size and topology design variables," *International Journal for Numerical Methods in Engineering*, vol. 117, no. 3, pp. 291–315, 2019.

[5] T. Liu, G. Sun, J. Fang, J. Zhang, and Q. Li, "Topographical design of stiffener layout for plates against blast loading using a modified ant colony optimization algorithm," *Structural and Multidisciplinary Optimization*, vol. 59, no. 2, pp. 335–350, 2019.

[6] D. Trias Mansilla, L. Marín Hernández, and M. Majó, "A comparative study of genetic algorithms for the multi-objective optimization of composite stringers under compression loads," *Composites Part B: Engineering*, vol. 47, pp. 130–136, 2013.

[7] H. Gao, J. Sun, W. Chen, Y. Zhang, and Q. Wu, "Structural bionic design for a machine tool column based on leaf veins," *Proceedings of the Institution of Mechanical Engineers, Part C: Journal of Mechanical Engineering Science*, vol. 232, no. 16, pp. 2764–2773, 2018.

[8] L. Zhao, J. Ma, W. Chen, and H. Guo, "Lightweight design and verification of gantry machining center crossbeam based on structural bionics," *Journal of Bionic Engineering*, vol. 8, no. 2, pp. 201–206, 2011.

[9] H. Zhang, X. Ding, X. Dong, and M. Xiong, "Optimal topology design of internal stiffeners for machine pedestal structures using biological branching phenomena," *Structural and Multidisciplinary Optimization*, vol. 57, no. 6, pp. 2323–2338, 2018.

[10] X. Dong, X. H. Ding, and M. Xiong, "Optimal layout of internal stiffeners for three-dimensional box structures based on natural branching phenomena," *Engineering Optimization*, vol. 51, no. 4, pp. 590–607, 2019.

[11] B. T. Li, J. Hong, S. N. Yan, and Z. F. Liu, "Multidiscipline topology optimization of stiffened plate/shell structures inspired by growth mechanisms of leaf veins in nature," *Mathematical Problems in Engineering*, vol. 201311 pages, Article ID 653895, 2013.

[12] S. Yan, B. T. Li, and J. Hong, "Bionic design and verification of high-precision machine tool structures," *International Journal of Advanced Manufacturing Technology*, vol. 81, no. 1–4, pp. 73–85, 2015.

[13] O. Sigmund and K. Maute, "Topology optimization approaches," *Structural and Multidisciplinary Optimization*, vol. 48, no. 6, pp. 1031–1055, 2013.

[14] L. Xia, L. Zhang, Q. Xia, and T. Shi, "Stress-based topology optimization using bi-directional evolutionary structural optimization method," *Computer Methods in Applied Mechanics and Engineering*, vol. 333, pp. 356–370, 2018.

[15] T. Kunakote and S. Bureerat, "Multi-objective topology optimization using evolutionary algorithms," *Engineering Optimization*, vol. 43, no. 5, pp. 541–557, 2011.

[16] D. Qin and Q. Zhu, "Structural topology optimization of box girder based on method of moving asymptotes (MMA)," in *Proceedings of the 2010 International Conference on Intelligent Computation Technology and Automation*, pp. 402–405, Changsha, China, May 2010.

[17] K. D. Tsavdaridis, J. J. Kingman, and V. V. Toropov, "Application of structural topology optimisation to perforated steel beams," *Computers & Structures*, vol. 158, pp. 108–123, 2015.

[18] Y.-S. Eom, K.-S. Yoo, J.-Y. Park, and S.-Y. Han, "Reliability-based topology optimization using a standard response surface method for three-dimensional structures," *Structural and Multidisciplinary Optimization*, vol. 43, no. 2, pp. 287–295, 2011.

[19] J. Liu, Y. Ma, A. J. Qureshi, and R. Ahmad, "Light-weight shape and topology optimization with hybrid deposition path planning for FDM parts," *International Journal of Advanced Manufacturing Technology*, vol. 97, no. 1–4, pp. 1123–1135, 2018.

[20] Z. L. Zhou, J. Song, and M. Cong, "Structure topology optimization of the spindle box of a machining center," *Advanced Materials Research*, vol. 421, pp. 225–229, 2011.

[21] Y. Yang, C. D. Moen, and J. K. Guest, "Three-dimensional force flow paths and reinforcement design in concrete via stress-dependent truss-continuum topology optimization,"

Journal of Engineering Mechanics, vol. 141, no. 1, Article ID 04014106, 2015.

[22] T. E. Johnson and A. T. Gaynor, "Three-dimensional projection-based topology optimization for prescribed-angle self-supporting additively manufactured structures," *Additive Manufacturing*, vol. 24, pp. 667–686, 2018.

[23] R. H. Zuberi, Z. X. Zuo, K. Long, and W. Li, "Topological optimization of constant beam section under moving load condition," in *Proceedings of the International Conference on Mechanic Automation and Control Engineering*, Wuhan, China, June 2010.

[24] F. Wu, Z. Wang, J. Han, and G. Pei, "Research on multi-objective topology optimization of diesel engine cylinder block based on analytic hierarchy process," *Mathematical Problems in Engineering*, vol. 2019, Article ID 6194634, 16 pages, 2019.

[25] A. Li, C. Liu, and S. Feng, "Topology and thickness optimization of an indenter under stress and stiffness constraints," *Journal of Mechanical Science and Technology*, vol. 32, no. 1, pp. 211–222, 2018.

[26] Q. Zhao, X. Chen, Z.-D. Ma, and Y. Lin, "Robust topology optimization based on stochastic collocation methods under loading uncertainties," *Mathematical Problems in Engineering*, vol. 2015, Article ID 580980, 14 pages, 2015.

[27] K. Liu and A. Tovar, "An efficient 3D topology optimization code written in Matlab," *Structural and Multidisciplinary Optimization*, vol. 50, no. 6, pp. 1175–1196, 2014.

[28] M. P. Bendsøe, *Topology Optimization: Theory, Methods, and Applications*, pp. 1–370, Springer, Berlin, Germany, 2004.

[29] G. Zhao, J. Liu, H. X. Wang, X. F. Yang, and G. L. Wen, "Strategy of sensitivity hierarchical filtering for overcoming load sickness phenomenon of continuum topology optimization," *Journal of Hunan University (Natural Sciences)*, vol. 8, pp. 79–85, 2018.

[30] D. Xiao, H. Zhang, X. Liu, T. He, and Y. Shan, "Novel steel wheel design based on multi-objective topology optimization," *Journal of Mechanical Science and Technology*, vol. 28, no. 3, pp. 1007–1016, 2014.